arXiv:quant-ph/0412002v1 1 Dec 2004

A new mechanism for electron spin echo envelope modulation

John J. L. Morton,[1,*] Alexei M. Tyryshkin,[2] Arzhang Ardavan,[3]
Kyriakos Porfyrakis,[1] Stephen A. Lyon,[2] and G. Andrew D. Briggs[1]

[1]*Department of Materials, Oxford University, Oxford OX1 3PH, United Kingdom*

[2]*Department of Electrical Engineering, Princeton University, Princeton, NJ 08544, USA*

[3]*Clarendon Laboratory, Department of Physics, Oxford University, Oxford OX1 3PU, United Kingdom*

(Dated: February 1, 2008)

Abstract

Electron spin echo envelope modulation (ESEEM) has been observed for the first time from a coupled *hetero*-spin pair of electron and nucleus in liquid solution. Previously, modulation effects in spin echo experiments have only been described in liquid solutions for a coupled pair of homonuclear spins in NMR or a pair of resonant electron spins in EPR. We observe low-frequency ESEEM (26 and 52 kHz) due to a new mechanism present for any electron spin with $S > 1/2$ that is hyperfine coupled to a nuclear spin. In our case these are electron spin ($S = 3/2$) and nuclear spin ($I = 1$) in the endohedral fullerene N@C_{60}. The modulation is shown to arise from second order effects in the isotropic hyperfine coupling of an electron and ^{14}N nucleus.

*Electronic address: john.morton@materials.ox.ac.uk

I. INTRODUCTION

Measuring the modulation of a spin echo in pulsed magnetic resonance experiments has become a popular technique for studying weak spin-spin couplings. It is used extensively in the fields of chemistry, biochemistry, and materials science, both in liquids and solids, using nuclear magnetic resonance (NMR) and electron paramagnetic resonance (EPR) [1, 2, 3]. Two distinct mechanisms for spin echo modulation have been identified in the literature.

In the first mechanism, a pair of spins, S and I, are coupled through an exchange or dipole-dipole interaction, $J\cdot\vec{S}\cdot\vec{I}$ or $J\cdot S_zI_z$, and the echo modulation arises for non-selective refocusing pulses which flip both coupled spins. The magnitude of the echo signal oscillates as $\cos(Jt)$, where t is the interpulse delay time ([4], page 500). This is most commonly observed for coupled pairs of homonuclear spins [5], though it is also known for pairs of coupled electron spins with identical or similar Larmor frequencies [6, 7].

It should be emphasised that a similar coupling, $J\cdot\vec{S}\cdot\vec{I}$, between unlike spins (including coupling between heteronuclear spins, hyperfine coupling between electron and nuclear spins, and electron-electron coupling between two electron spins with different Larmor frequencies) results in no modulation effects from this mechanism: The hetero-spin coupling energy changes its sign upon application of the refocusing pulse (because only one spin flips), and the magnetization is thus fully refocused at the time of echo formation, in the same way as in the presence of any other inhomogeneous magnetic fields.

A second ESEEM mechanism, which does apply to coupled pairs of hetero-spins, has also been identified [2, 3]. This mechanism requires *anisotropic* spin-spin interactions (e.g. $A_{zz}S_zI_z + A_{zx}S_zI_x$) and is therefore restricted to solids or high viscosity liquids. The modulation arises as a result of "branching" of the spin transitions created by the refocusing pulse. The resonant spin S precesses with Larmor frequency that is different before and after the refocusing pulse and therefore accumulates an additional phase which causes oscillations in the echo signal, as $\cos(\omega_{Ik}t)$, where ω_{Ik} is the spin transition frequency of the non-resonant spin I. The amplitude of the oscillations depends on magnitude of the anisotropic hyperfine component.

In this Paper we demonstrate that, contrary to previous belief, echo modulation effects can also be observed for a hetero-spin pair coupled by a purely *isotropic* spin interaction, and we thus identify a new ESEEM mechanism. Our hetero-spin pair is the endohedral fullerene

$N@C_{60}$ in CS_2 solution, with electron spin $S = 3/2$ interacting through an isotropic hyperfine coupling ($a\cdot\vec{S}\cdot\vec{I}$, $a = 15.8$ MHz) to the nuclear spin $I = 1$ of ^{14}N. The isotropic hyperfine coupling lifts the degeneracy of the electron spin transitions, leading to a profound modulation of the echo intensity at about 52 kHz. We shall show that this third modulation mechanism is only effective in high-spin electron systems ($S > 1/2$). The $N@C_{60}$ molecule has an exceptionally long electron spin dephasing time ($T_2 = 210$ μs), enabling the observation of this low frequency ESEEM for the first time.

II. MATERIALS AND METHODS

High-purity endohedral $N@C_{60}$ was prepared [8], dissolved in CS_2 to a final concentration of 1-2$\cdot 10^{15}$/cm^3, freeze-pumped in three cycles to remove oxygen, and finally sealed in a quartz EPR tube. Samples were 0.7-1.4 cm long, and contained approximately $5 \cdot 10^{13}$ $N@C_{60}$ spins. Pulsed EPR measurements were done at 190 K using an X-band Bruker Elexsys580e spectrometer, equipped with a nitrogen-flow cryostat. In the 2-pulse (Hahn) electron spin echo (ESE) experiments, $\pi/2-\tau-\pi-\tau-echo$, the $\pi/2$ and π pulse durations were 56 and 112 ns respectively. Phase cycling was used to eliminate the contribution of unwanted free induction decay (FID) signals.

III. RESULTS AND DISCUSSION

Fig. 1(A) shows the continuous-wave EPR spectrum of $N@C_{60}$ in CS_2 at room temperature. The spectrum is centered on the electron g-factor $g = 2.0036$ and comprises three lines resulting from the hyperfine coupling to ^{14}N [9]. The relevant isotropic spin Hamiltonian (in angular frequency units) is:

$$\mathcal{H}_0 = \omega_e S_z - \omega_I I_z + a\cdot\vec{S}\cdot\vec{I}, \tag{1}$$

where $\omega_e = g\beta B_0/\hbar$ and $\omega_I = g_I\beta_n B_0/\hbar$ are the electron and ^{14}N nuclear Zeeman frequencies, g and g_I are the electron and nuclear g-factors, β and β_n are the Bohr and nuclear magnetons, $\hbar$ is Planck's constant and B_0 is the magnetic field applied along z-axis in the laboratory frame. Each hyperfine line (marked in Fig. 1(A) with $M_I = 0$ and ± 1) involves the three allowed electron spin transitions $\Delta M_S = 1$ within the $S = 3/2$ multiplet. These electron

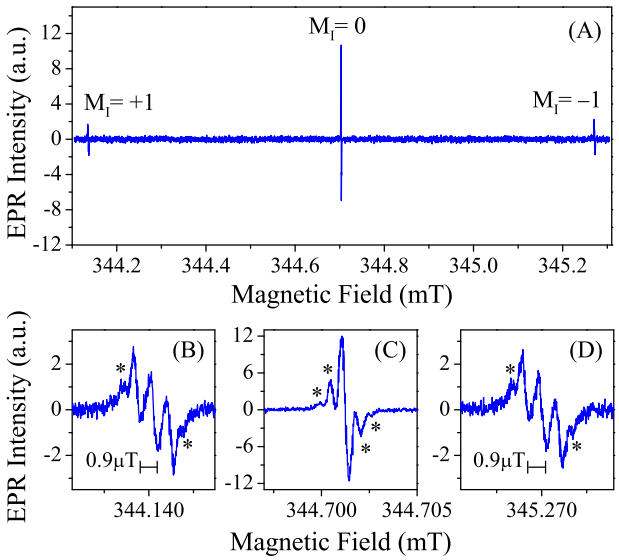

FIG. 1: (A) EPR spectrum of N@C_{60} in CS_2 at room temperature. Each line in the triplet signal is labeled with the corresponding projection M_I of the ^{14}N nuclear spin. (B-D) Zoom-in for each line showing details of the lineshape structure. Small satellite lines (marked with $*$) are due to a hyperfine interaction with the natural abundance of ^{13}C nuclei on the C_{60} cage. Measurement parameters: microwave frequency, 9.67 GHz; microwave power, 0.5 μW; modulation amplitude, 2 mG; modulation frequency, 1.6 kHz.

spin transitions remain degenerate for $M_I = 0$ as seen in Fig. 1(C) but split into three lines (with relative intensities 3:4:3) for $M_I = \pm 1$, as seen in Figs. 1(B) and (D). This additional splitting of 0.9 μT originates from the second order hyperfine corrections $a^2/\omega_e = 26$ kHz, and its observation is only possible because of the extremely narrow EPR linewidth < 0.3 μT in N@C_{60}. Similar second-order splittings have been reported for the related spin system of endohedral fullerene ^{31}P@C_{60} which has $S = 3/2$ coupled with $I = 1/2$ [10].

Fig. 2(A) shows two-pulse echo decays measured at the central $M_I = 0$ and the high-field $M_I = -1$ hyperfine lines. The decay is monotonic for $M_I = 0$ and has an exponential dependence $\exp(-2\tau/T_2)$ with $T_2 = 210$ μs. However, the decay is oscillatory for $M_I = -1$ (and also for $M_I = +1$, not shown) — the Fourier transform of the decay reveals two peaks at frequencies 26 and 52 kHz as seen in Fig. 2(B). These frequencies correlate closely to the splitting of 26 kHz found in the EPR spectrum in Fig. 1(B) and (D), indicating that the two effects have the same origin.

We shall use the spin density operator formalism to derive the modulation effects for the

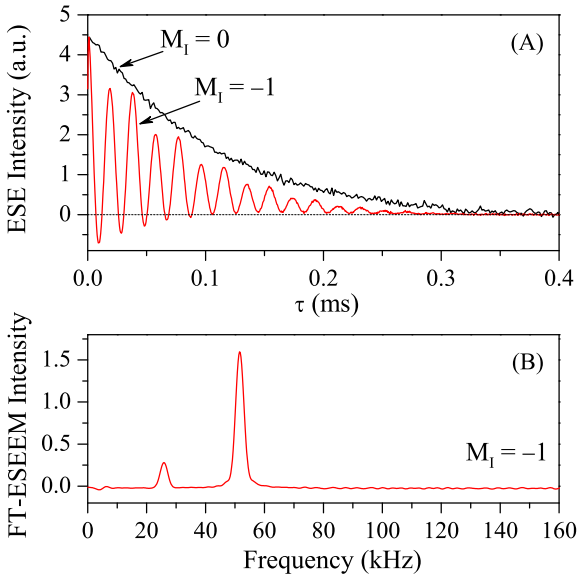

FIG. 2: (A) Two-pulse ESE decays for N@C_{60} in CS_2 at 190 K measured at the central $M_I = 0$ and the high-field $M_I = -1$ hyperfine components of the EPR spectrum. (B) The Fourier Transform (FT) of the oscillatory echo decay at $M_I = -1$.

spin system $S = 3/2$, $I = 1$. The spin density matrix after our two-pulse echo experiment is given by

$$\sigma(\tau) = (U_\tau R_2^x U_\tau R_1^x) \cdot \sigma_0 \cdot (U_\tau R_2^x U_\tau R_1^x)^\dagger. \tag{2}$$

Here, σ_0 is the density matrix at thermal equilibrium; in the high-temperature approximation valid in our experiments, σ_0 can be substituted with a spin operator S_z [3]. The evolution operator $U_\tau = \exp(-i\mathcal{H}_0\tau)$ describes a free evolution of the spin system between the applied microwave pulses, and the spin rotation operators, R_i^x, describe spin rotation upon application of the two microwave pulses, $i = 1, 2$. The measured echo intensity is

$$V(\tau) = \mathrm{Tr}\left[\sigma(\tau) \cdot D\right]. \tag{3}$$

The detection operator $D = S_y \otimes \mathcal{P}_{M_I}$ involves the ^{14}N nuclear spin projection operator $\mathcal{P}_{M_I}$ to selectively detect only those spin transitions associated with a specific nuclear spin projection M_I. In a pulsed EPR experiment, this corresponds to performing measurements at the resolved hyperfine line in the EPR spectrum of N@C_{60} and integrating over the echo signal shape to average out oscillating signals from other off-resonance hyperfine lines. The

echo derives from a sum of the single quantum (SQ) coherences (represented by the terms $\sigma_{n,n+1}$ and $\sigma_{n+1,n}$ in the density matrix), weighted by factors from the detection operator D.

Our Hamiltonian, $\mathcal{H}_0$ (Eq. 1), has small off-diagonal elements provided by the $a(I_xS_x + I_yS_y)$ terms. These terms are often omitted since they are known to contribute only second order energy corrections [4, 11], but are, in fact, directly responsible for the observed ESEEM. Diagonalisation of Eq. 1 yields the magnitude of these corrections to be of order $\delta = a^2/\omega_e$, consistent with the splitting observed in Fig. 1(B) and (D). In addition, the isotropic hyperfine interaction introduces a small degree of mixing between I_z, S_z basis states, however we find that this small mixing need not be considered to appreciate the origin of the observed ESEEM. With this assumption, our Hamiltonian and all other operators have block-diagonal structures with non-zero elements only between states with the same M_I. Transitions with simultaneous flip of both electron and nuclear spins are thus forbidden [12] and the evolution of electron spin can be treated individually for each nuclear spin manifold. We can therefore avoid the derivation in the full 12×12 Hilbert space in a general form, and instead reduce the dimensionality to 4×4. The validity of this approximation is confirmed below by a rigorous derivation using Average Hamiltonian Theory. The reduced $M_I = +1$ subspace of the diagonalised Hamiltonian, correct to second order in a, becomes:

$$\mathcal{H}_0 = S_z(\omega_e + a) - I_z\omega_I - \begin{pmatrix} 0 & 0 & 0 & 0 \\ 0 & \frac{3\delta}{2} & 0 & 0 \\ 0 & 0 & 2\delta & 0 \\ 0 & 0 & 0 & \frac{3\delta}{2} \end{pmatrix}, \tag{4}$$

which we can rearrange as:

$$\mathcal{H}_0 = S_z(\omega_e + a + \frac{\delta}{2}) - I_z(\omega_I + \frac{7\delta}{4}) + \begin{pmatrix} \delta & 0 & 0 & 0 \\ 0 & 0 & 0 & 0 \\ 0 & 0 & 0 & 0 \\ 0 & 0 & 0 & \delta \end{pmatrix} I_z. \tag{5}$$

The term $-I_z(\omega_I + 7/4\delta)$ represents a constant energy shift and can be ignored. We move into a resonant rotating frame (the coordinate system rotating with the microwave frequency ω_{mw} around the laboratory z-axis). In this frame the spin Hamiltonian (4) transforms to $\mathcal{H} - \omega_{mw}S_z$, such that:

$$\mathcal{H}_0 = \begin{pmatrix} 3/2\Delta + \delta & 0 & 0 & 0 \\ 0 & 1/2\Delta & 0 & 0 \\ 0 & 0 & -1/2\Delta & 0 \\ 0 & 0 & 0 & -3/2\Delta + \delta \end{pmatrix}, \tag{6}$$

where $\Delta = \omega_e + a + \delta/2 - \omega_{mw}$ is the resonance offset frequency.

The rotation operator $R_i^x = \exp(-i(\mathcal{H}_0 + \mathcal{H}_1)t_{p_i})$ can be simplified by taking into account a finite excitation bandwidth of the microwave pulses, which are selective upon one hyperfine line in the EPR spectrum. $\mathcal{H}_1 = g\beta B_1 S_x/\hbar$ where B_1 is the microwave magnetic field applied along x-axis in the rotating frame and t_{p_i} is the duration of the microwave pulses. Furthermore, since the bandwidth of $B_1 \simeq 4.5$ MHz is large compared to both the intrinsic EPR linewidth 9 kHz and the second-order spitting 26 kHz of the outer lines in the EPR spectrum, all three spin transitions within electron the $S = 3/2$ multiplet are equally excited and the respective rotating operator can be approximated as $R_i^x \simeq \exp(-i\mathcal{H}_1 t_{p_i}) = \exp(-i\theta_i S_x)$, where $\theta_i = g\beta B_1 t_{p_i}/\hbar$ is the microwave pulse rotation angle. This results in the following spin rotation operator for an on-resonance hyperfine line:

$$R_i^x = \begin{pmatrix} \cos^3\frac{\theta_i}{2} & \frac{i}{\sqrt{3}}(\sin^3\frac{\theta_i}{2} + \sin\frac{3\theta_i}{2}) & -\frac{1}{\sqrt{3}}(\cos^3\frac{\theta_i}{2} - \cos\frac{3\theta_i}{2}) & -i\sin^3\frac{\theta_i}{2} \\ \frac{i}{\sqrt{3}}(\sin^3\frac{\theta_i}{2} + \sin\frac{3\theta_i}{2}) & \frac{1}{3}(\cos^3\frac{\theta_i}{2} + 2\cos\frac{3\theta_i}{2}) & -\frac{i}{3}(\sin^3\frac{\theta_i}{2} - 2\sin\frac{3\theta_i}{2}) & -\frac{1}{\sqrt{3}}(\cos^3\frac{\theta_i}{2} - \cos\frac{3\theta_i}{2}) \\ -\frac{1}{\sqrt{3}}(\cos^3\frac{\theta_i}{2} - \cos\frac{3\theta_i}{2}) & -\frac{i}{3}(\sin^3\frac{\theta_i}{2} - 2\sin\frac{3\theta_i}{2}) & \frac{1}{3}(\cos^3\frac{\theta_i}{2} + 2\cos\frac{3\theta_i}{2}) & \frac{i}{\sqrt{3}}(\sin^3\frac{\theta_i}{2} + \sin\frac{3\theta_i}{2}) \\ -i\sin^3\frac{\theta_i}{2} & -\frac{1}{\sqrt{3}}(\cos^3\frac{\theta_i}{2} - \cos\frac{3\theta_i}{2}) & \frac{i}{\sqrt{3}}(\sin^3\frac{\theta_i}{2} + \sin\frac{3\theta_i}{2}) & \cos^3\frac{\theta_i}{2} \end{pmatrix}. \tag{7}$$

We need not consider the rotation operator for off-resonance lines, as their excitation will lead to an oscillating echo signal which is averaged out by selective detection (i.e. through the detection operator D) and therefore does not contribute to the overall echo signal.

We evaluate Eq. 2 for the two-pulse echo experiment $\pi/2 - \tau - \pi - \tau - echo$, and rearrange terms for the purposes of the discussion which follows:

$$\sigma(\tau) = (U_\tau R_\pi^x U_\tau) \cdot (R_{\pi/2}^x \cdot \sigma_0 \cdot (R_{\pi/2}^x)^\dagger) \cdot (U_\tau R_\pi^x U_\tau)^\dagger. \tag{8}$$

Evaluating the heart of the echo sequence, $U_\tau R_\pi^x U_\tau$, is instructive in understanding the source of the observed modulation. From Eq. 7, a perfect π rotation is:

$$R_{\pi}^{x} = \begin{pmatrix} 0 & 0 & 0 & -i \\ 0 & 0 & -i & 0 \\ 0 & -i & 0 & 0 \\ -i & 0 & 0 & 0 \end{pmatrix}, \tag{9}$$

with the resulting echo sequence operator shown below.

$$U_{\tau} R_{\pi}^{x} U_{\tau} = -i \begin{pmatrix} 0 & 0 & 0 & e^{2i\delta t} \\ 0 & 0 & 1 & 0 \\ 0 & 1 & 0 & 0 \\ e^{2i\delta t} & 0 & 0 & 0 \end{pmatrix} \tag{10}$$

This indicates that over the course of the experiment, states $S = \pm 3/2$ pick up a phase of $2\delta t$ with respect to the states $S = \pm 1/2$, or in other words, the outer SQ coherences ($\sigma_{1,2}, \sigma_{2,1}, \sigma_{3,4}$ and $\sigma_{4,3}$) oscillate with frequency 2δ, while the phases of the inner SQ coherences ($\sigma_{2,3}$ and $\sigma_{3,2}$) remain constant.

The initial SQ coherences are provided by the first rotation ($\pi/2$):

$$R_{\pi/2}^{x} \cdot \sigma_0 \cdot (R_{\pi/2}^{x})^{\dagger} = \begin{pmatrix} 0 & -i\sqrt{3}/2 & 0 & 0 \\ i\sqrt{3}/2 & 0 & -i & 0 \\ 0 & i & 0 & -i\sqrt{3}/2 \\ 0 & 0 & i\sqrt{3}/2 & 0 \end{pmatrix}, \tag{11}$$

and the measuring weighting factors for each coherence are: $\sqrt{3}/2$, 1, and $\sqrt{3}/2$ (associated with the detection operator $\mathcal{D}$). Together these imply that the three coherences contribute to the measured echo intensity with relative amplitudes 3:4:3. In other words, their sum will yield a constant component, and one oscillating with frequency 2δ, with respective amplitudes 4:6. This is confirmed upon evaluation of Eq. 3,

$$V_{M_I=\pm 1}(\tau) = 2 + 3\cos 2\delta\tau, \tag{12}$$

and is consistent with the observed echo in Fig. 2B. The modulation amplitude is deep and the echo signal can change its sign at the minima.

The effect is illustrated in Fig. 3(A), which shows the phases gained during the "defocusing" period τ, i.e. free evolution after the initial pulse θ_1 and before the refocusing pulse

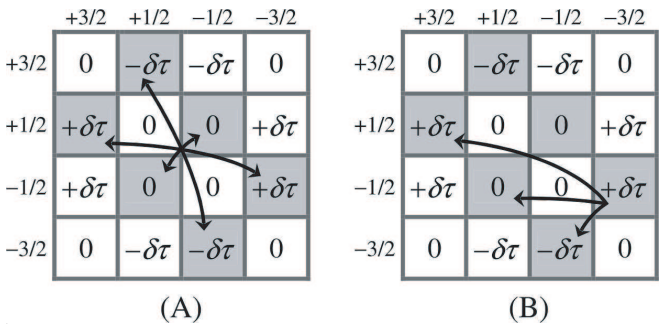

FIG. 3: Phases gained by the density matrix elements during the 2-pulse ESE experiment at $M_I = +1$. Phases caused by off-resonance refocus fully and are therefore omitted for clarity. The shaded off-diagonal elements represent single-quantum (SQ) coherences which generate the echo signal upon refocusing. In (A) the arrows indicate the transition between the SQ coherences caused by a perfect refocusing pulse with $\theta_2 = \pi$. (B) shows all possible transitions (spin coherence branching), for one SQ coherence element, caused by an imperfect refocusing pulse with $\theta_2 \neq \pi$.

θ_2. These phases derive from the differences between adjacent elements along the diagonal of the Hamiltonian in Eq. 6 (the off-resonance, Δ, is ignored as it is fully canceled upon echo formation). The six SQ coherence elements, shaded in the Figure and responsible for echo formation, gain the phases 0 or $\pm\delta\tau$. Upon application of the perfect refocusing pulse with $\theta_2 = \pi$ each SQ coherence element uniquely transforms, as shown with arrows, and continues to evolve during the "refocusing" period τ to gain an additional phase which does not compensate, but instead doubles, the initial phase. Thus, at time of echo formation the SQ coherences arrive with three different phases 0 and $\pm 2\delta\tau$. Their vector sum interferes destructively to produce an echo signal whose magnitude oscillates as $2\delta\tau$ in accordance with Eq. 12.

The case of an imperfect refocusing pulse with $\theta_2 \neq \pi$ is shown in Fig. 3(B). In contrast to $\theta_2 = \pi$ with a one-to-one transformation of each density matrix element, the non-ideal pulse generates branching of the electron spin transitions. Therefore, the SQ coherence element which initially gained the phase $+\delta\tau$ during the "defocusing" period, refocuses into three SQ coherences (shown with the arrows), each accumulating different phases during the "refocusing" period. Thus, at the time of echo formation the accumulated phases are 0, $+\delta\tau$, and $+2\delta\tau$. The vector sum of these and other SQ coherences produces a complex interference with the echo signal oscillating with two frequencies δ and 2δ as observed in Fig. 2. Thus,

the second harmonic δ found in the echo modulation is the result of an imperfect refocusing pulse.

The preceeding physical description provides an intuitive view of the new ESEEM effect. For it to be fully rigorous, however, we should consider the effect of the mixing of the I_z, S_z basis states. This necessarily involves the full 12-dimensional Hilbert space and the argument rapidly becomes opaque. Fortunately, the same results can be rigorously obtained from the first order correction in Average Hamiltonian Theory (AHT) [13], which is equivalent to a standard perturbation theory approach in the rotating frame.

We begin by transforming the original Hamiltonian (Eq. (1)) into a rotating frame of angular frequency ω_{mw}, defining Ω_e as the deviation from the electron Larmor frequency, $\Omega_e = \omega_e - \omega_{mw}$,

$$\begin{aligned} \mathcal{H}_0 &= \Omega_e S_z - \omega_I I_z + a[S_z I_z + S_x I_x \cos(\omega_{mw} t) \\ &\quad - S_y I_y \sin(\omega_{mw} t)]. \end{aligned} \tag{13}$$

The oscillatory terms in Eq. 13 are averaged out in the zeroth-order average Hamiltonian:

$$\overline{\mathcal{H}}_0^{(0)} = \Omega_e S_z - \omega_I I_z + a S_z I_z. \tag{14}$$

Here, the bar over $\mathcal{H}_0$ refers to an average over one period of the oscillation ω_{mw}. As the Hamiltonian in Eq. (14) results in no modulation of the echo signal for a coupled hetero-spin pair, the higher order terms of the average Hamiltonian must be included (see, for example, Ref. [3], p.83). The first order correction is:

$$\overline{\mathcal{H}}_0^{(1)} = \frac{\delta}{2}\left[\left(I(I+1) - I_z^2\right) S_z - \left(S(S+1) - S_z^2\right) I_z\right]. \tag{15}$$

We find that the average Hamiltonian $\overline{\mathcal{H}}_0 = \overline{\mathcal{H}}_0^{(0)} + \overline{\mathcal{H}}_0^{(1)}$ is sufficient to describe the modulation effects. In this approach the time-dependent mixing terms have been properly accounted for to produce (after time averaging) the second order energy corrections in $\overline{\mathcal{H}}_0^{(1)}$. However, these mixing terms appear to average to zero, with the result that the effective Hamiltonian, $\overline{\mathcal{H}}_0$, is a diagonal matrix, thus validating our earlier qualitative approach.

It can also be verified that in the presence of the applied microwave field, the average Hamiltonian is, to first order, the simple sum $\overline{\mathcal{H}}_0 + g\beta B_1 S_x/\hbar$. Therefore, the rotation operator, R_i^x, and detection operator, D have the same block diagonal structures described

above (non-zero elements only within the same M_I subspace). This allows us again to reduce the dimensionality of the Hilbert space to 4×4.

Substituting Eqs. (7, 14 and 15) into Eq. (3), and after some manipulation, we find the following expressions for the echo amplitude in a general two-pulse sequence $\theta_1 - \tau - \theta_2 - \tau - echo$, for the $S = 3/2, I = 1$ spin system. The echo modulation is identical for the two outer $M_I = \pm 1$ hyperfine lines,

$$\begin{aligned} V_{M_I=\pm 1}(\tau) &= 2 \sin\theta_1 \sin^2 \frac{\theta_2}{2} [A_0(\theta_2) + A_1(\theta_2) \cos\delta\tau \\ &\quad + A_2(\theta_2) \cos 2\delta\tau], \end{aligned} \tag{16}$$

where

$$\begin{aligned} A_0(\theta_2) &= 1 - 6\cos^2\frac{\theta_2}{2} + \frac{27}{2}\cos^4\frac{\theta_2}{2}, \\ A_1(\theta_2) &= 6\cos^2\frac{\theta_2}{2}\left(2 - 3\cos^2\frac{\theta_2}{2}\right), \\ A_2(\theta_2) &= \frac{3}{2}\sin^2\frac{\theta_2}{2}\left(1 - 3\cos^2\frac{\theta_2}{2}\right), \end{aligned} \tag{17}$$

The signal is modulated with frequencies δ and 2δ, consistent with the experimental observations in Fig. 2. The modulation amplitudes in Eq. (17) depend strongly on the rotation angles of the microwave pulses. At optimal rotation angles, $\theta_1 = \pi/2, \theta_2 = \pi$, Eq. 12 is recovered.

In contrast to the two outer lines, the echo signal at the central $M_I = 0$ hyperfine line shows no modulation effects,

$$V_{M_I=0}(\tau) = 2\sin\theta_1 \sin^2\frac{\theta_2}{2}. \tag{18}$$

It is instructive to consider which terms in the average Hamiltonian $\overline{\mathcal{H}}_0^{(1)}$ give rise to the modulation effects. The terms $I(I+1)S_z$ and $S(S+1)I_z$ are not responsible as they produce only a constant shift to the electron and nuclear Zeeman frequencies, respectively. The term $I_z^2 S_z$ is also irrelevant because electron-nuclear flip-flop transitions are forbidden, hence M_I stays invariant during the experiment. This term changes its sign, but not its magnitude, during the refocusing pulse and thus fully refocuses. Therefore, $S_z^2 I_z$ is solely responsible for the modulation effects. For $M_I = 0$, this last term becomes zero and consequently there are no modulation effects produced at the central hyperfine line in the EPR spectrum. Note

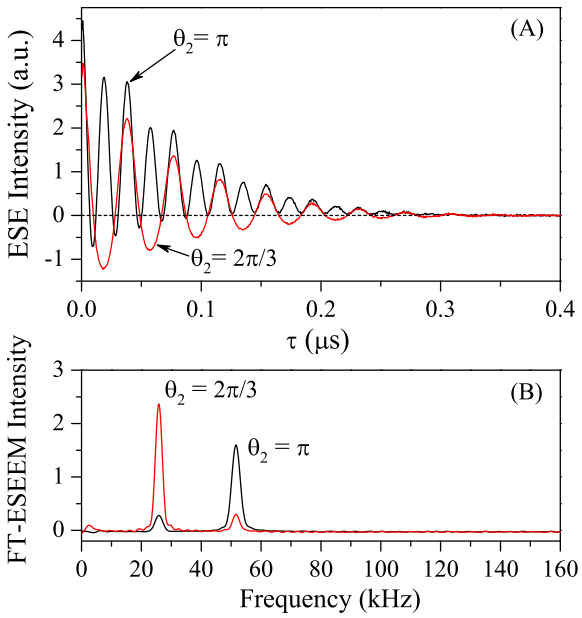

FIG. 4: Two-pulse ESE decays (A) and their Fourier Transform spectra (B) measured at hyperfine line $M_I = -1$ of the EPR spectrum, using the refocusing pulse $\theta_2 = \pi$ and $\theta_2 = 2\pi/3$. Other experimental conditions are the same as in Fig. 2

that this term is responsible for the *spin-dependent* shifts to the energies of the spin states used in the earlier derivation (see Eqs. 5 and 6).

The effect of a non-π refocusing pulse angle is shown in Fig. 4. As predicted by Eq. (16), we observe that when $\theta_2 = 2\pi/3$, the modulation effects are dominated by the low-frequency δ, rather than the high-frequency 2δ found when $\theta_2 = \pi$.

Eq. 16 also confirms that a perfect π refocusing pulse yields only a 2δ frequency component in the modulation, however, a δ component is clearly observed in Fig. 2. The imperfection is explained by the inhomogeneity of the microwave magnetic field B_1 in the resonator cavity which results in a distribution of spin rotation angles θ_2 across the ensemble. If we assume a Gaussian distribution of rotation angles, the relative intensities of the low- and high-frequency components $I_1/I_2 = 0.17$ in the experimental spectrum corresponds to a standard deviation of $\sigma = 0.31$ radians. This corresponds to a 10% error in a π rotation angle, consistent with previously reported values for B_1-field inhomogeneity in this resonator cavity [14]. To verify that the B_1 field inhomogeneity is the source of the low-frequency component, we applied an error-correcting composite π-pulse as the refocusing pulse. The resulting ESEEM contained only the single 52 kHz frequency component.

The derivation of the modulation is easily generalised to the case of an arbitrary electron spin $S > 1/2$ coupled through an isotropic hyperfine interaction to a magnetic nucleus. Using an approach similar to that described in Eqs. (9, 10 and 11), the general expression for 2-pulse ESEEM with a perfect refocusing pulse can be shown to be

$$V(\tau) = \sum_{M_S=-S}^{S} (S - M_S)(S + M_S + 1)\, e^{i(1+2M_S)M_I \delta\tau} \tag{19}$$

The summation is over electron spin projections M_S, whilst the nuclear spin projection M_I identifies the hyperfine line of the EPR spectrum in which the modulation effects are observed.

IV. CONCLUSIONS

Potential applications of this new mechanism include measuring the hyperfine coupling constant and determining electron spin number; it may also be relevant to certain quantum information processing schemes [15]. The accurate measurement of the hyperfine constant in a continuous-wave EPR measurement is subject to B_0 field instability (typically >10 mG). However, the ESEEM frequency can be measured accurately, given a sufficiently long dephasing time, potentially providing a more precise measurement. In this case accuracy may be improved by moving to lower applied magnetic fields (lower EPR frequency). In contrast with other types of ESEEM, this would also lead to a *higher* modulation frequency. Finally, we note that given appropriate electron-nuclear spin coupling energies and decoherence times, this effect will also lead to modulation in nuclear spin echo experiments.

V. ACKNOWLEDGEMENTS

We would like to thank Wolfgang Harneit's group at the Hahn-Meitner Institute for providing nitrogen-doped fullerenes, and John Dennis at Queen Mary's College, London, Martin Austwick and Gavin Morley for the purification of N@C_{60}. A Foresight LINK grant *Nanoelectronics at the quantum edge*, an EPSRC grant and the Oxford-Princeton Link fund supported this project. We thank Brendon Lovett for valuable discussions. AA is supported by the Royal Society. Work at Princeton was supported by the NSF International Office through the Princeton MRSEC Grant No. DMR-0213706 and by the ARO and ARDA under

Contract No. DAAD19-02-1-0040.

---

[1] R. R. Ernst, G. Bodenhausen, and A. Wokaun, *Principles of nuclear magnetic resonance in one and two dimensions*, The International series of monographs on chemistry ; 14 (Clarendon Press ; Oxford University Press, Oxford Oxfordshire New York, 1987).

[2] S. A. Dikanov and Y. D. Tsvetkov, *Electron spin echo envelope modulation (ESEEM) spectroscopy* (CRC Press, Boca Raton, 1992).

[3] A. Schweiger and G. Jeschke, *Principles of pulse electron paramagnetic resonance* (Oxford University Press, Oxford, UK ; New York, 2001).

[4] A. Abragam, *The principles of nuclear magnetism* (Clarendon Press, Oxford, 1961).

[5] E. L. Hahn and D. E. Maxwell, Phys. Rev. **88**, 1070 (1952).

[6] V. F. Yudanov, K. M. Salikhov, G. M. Zhidomirov, and Y. D. Tsvetkov, Teor. Eksp. Khim. **5**, 663 (1969).

[7] A. D. Milov and Y. D. Tsvetkov, Dokl. Akad. Nauk SSSR **288**, 924 (1986).

[8] M. Kanai, K. Porfyrakis, G. A. D. Briggs, and T. J. S. Dennis, Chem. Comm. pp. 210–211 (2004).

[9] T. Almeida-Murphy, T. Pawlik, A. Weidinger, M. Hohne, R. Alcala, and J. M. Spaeth, Phys. Rev. Lett. **77**, 1075 (1996).

[10] C. Knapp, N. Weiden, K. Kass, K. P. Dinse, B. Pietzak, M. Waiblinger, and A. Weidinger, Mol. Phys. **95**, 999 (1998).

[11] C. P. Slichter, *Principles of magnetic resonance* (Springer, Berlin, 1996), 3rd ed.

[12] These flip-flop transitions are allowed only to third order - the transition probability is proportional to a^2/ω_e^3 and thus is negligibly small at $a = 15.8$ MHz for N@C_{60}.

[13] U. Haeberlen and J. Waugh, Phys. Rev. **125**, 453 (1968).

[14] J. J. L. Morton, A. M. Tyryshkin, A. Ardavan, K. Porfyrakis, S. A. Lyon, and G. A. D. Briggs, Phys. Rev. A, *in press*, quant-ph/0403226.

[15] The N@C_{60} molecule has been proposed as an electron spin-based qubit in several quantum information processing schemes [**?** **?**]. At the very least, the slow evolution within the sublevels of the $S = 3/2$ system which is responsible for the observed ESEEM must be taken into account when designing pulse sequences to perform a quantum algorithm. However, it

could also be exploited to provide a separate family of gates for performing operations between sublevels, increasing the potential of $N@C_{60}$ as a single quantum bit.